

Convective heat transport in stratified atmospheres at low and high Mach number

Evan H. Anders and Benjamin P. Brown

*Department of Astrophysical & Planetary Sciences, University of Colorado – Boulder and
Laboratory for Atmospheric and Space Physics, Boulder, CO*

Convection in astrophysical systems is stratified and often occurs at high Rayleigh number (Ra) and low Mach number (Ma). Here we study stratified convection in the context of plane-parallel, polytropically stratified atmospheres. We hold the density stratification (n_ρ), aspect ratio, and Prandtl number (Pr) constant while varying the superadiabaticity and Ra. We find that Ma is a strong function of the superadiabaticity in both 2D and 3D simulations, and that it is a weak function of Ra in 2D. In 2D simulations, the scaling of the Nusselt Number (Nu) and the Reynolds number (Re) with Ra weaken once the mean Ma of the solution is unity, but in 3D Re and Nu seem to have consistent scaling across Ra. We further find that when the superadiabaticity and Ma are large, density inversions form in the thermal boundary layers.

INTRODUCTION

Convection transports energy in stellar and planetary atmospheres. In these objects, flows are compressible and feel the atmospheric stratification. While in some systems this stratification is negligible, it is significant in regions such as the convective envelope of the Sun, which spans 14 density scale heights. In the bulk of these systems, flows are at very low Mach number (Ma), but numerical constraints have restricted most studies of compressible convection to high Ma. These prior studies have provided important insight into the low temperature, high Ma region near the Sun’s surface. Few fundamental properties of low Ma convection, which characterizes deeper motions, are known.

In the widely-studied Rayleigh-Bénard (RB) problem of incompressible Boussinesq convection, a negative temperature gradient leads to convective instability. In the evolved solution, upflows and downflows are symmetrical, the temperature in the interior becomes isothermal and the conductive flux ($\propto \nabla T$) approaches zero there. For compressible convection in a stratified atmosphere, a negative entropy gradient leads to convective instability. Early numerical experiments of moderate-to-high Ma compressible convection in two [1–4] and three [5, 6] dimensions revealed that the evolved state differs from the RB case. Downflow lanes become fast and narrow, and upflow lanes turn into broad, slow upwellings. Furthermore, the *entropy* gradient is negated by convection in the interior, and a significant temperature gradient and conductive flux persist in the presence of efficient convection.

In RB convection, there exist two primary dynamical control parameters: the Rayleigh number (Ra, the ratio of buoyant driving to diffusive damping) and the Prandtl number (Pr, the ratio of viscous to thermal diffusivity). These numbers control two useful measures of turbulence in the evolved solution: the Reynolds number (Re, the strength of advection to viscous diffusion) and the Peclet number (Pe, advection vs. thermal diffusion). In stratified atmospheres, the magnitude of the unstable entropy

gradient, joins Ra and Pr as an important control parameter. This *superadiabatic excess* [1], ϵ , sets the scale of the atmospheric entropy gradient. We find here that ϵ primarily controls the Ma of the evolved solution.

In this letter we study the behavior of convective heat transport, quantified by the Nusselt number (Nu), in plane-parallel, two- and three-dimensional, polytropically stratified atmospheres. We vary ϵ and Ra while holding Pr, aspect ratio, boundary conditions, and initial atmospheric stratification constant. We also examine the behavior of flow properties, as quantified by Ma and Re.

EXPERIMENT

We examine a monatomic ideal gas with an adiabatic index of $\gamma = 5/3$ whose equation of state is $P = R\rho T$. In this work we take $R = 1$. This is consistent with the approach used in earlier work [1–6] and is the simplest stratified extension of RB. We study atmospheres which are initially polytropically stratified,

$$\begin{aligned}\rho_0(z) &= \rho_t(1 + L_z - z)^m, \\ T_0(z) &= T_t(1 + L_z - z),\end{aligned}\quad (1)$$

where m is the polytropic index and L_z is the depth of the atmosphere. Subscript 0 indicates initial conditions and subscript t indicates values at $z = L_z$. The height coordinate, z , increases upwards in the range $[0, L_z]$. We specify the depth of the atmosphere, $L_z = e^{n_\rho/m} - 1$, by choosing the number of density scale heights, n_ρ , it spans initially. Throughout this letter we set $n_\rho = 3$. Satisfying hydrostatic equilibrium sets the value of gravity, $g = T_t(m + 1)$, which is constant with depth. We study atmospheres with aspect ratios of 4 where both the x and y coordinates have the range $[0, 4L_z]$. In our 2D cases, we only consider x and z .

Convective dynamics are controlled by the superadiabaticity of the atmospheres as well as the atmospheric diffusivities. The superadiabaticity, or the magnitude of the (negative) entropy gradient, is set by the superadiabatic excess, $\epsilon = m_{ad} - m$, where $m_{ad} = (\gamma - 1)^{-1}$.

The atmospheric thermal diffusivity, χ , and kinematic viscosity (viscous diffusivity), ν , are determined by the Rayleigh number (Ra) and the Prandtl number (Pr). We set $\text{Pr} = \nu/\chi = 1$ throughout this work. The polytropic initial conditions are in thermal equilibrium, $\kappa_0 \partial_z T_0 = \text{const}$, so $\kappa_0 = \chi \rho_0$ must be constant. To keep Pr constant with height, we set $\chi = \chi_t / \rho_0$ and $\nu = \nu_t / \rho_0$. Under these constraints, the diffusivity profiles are specified by choosing Ra at the top of the domain,

$$\text{Ra}_{\text{top}} = \frac{gL_z^3(\Delta S_0/c_P)}{\nu_t \chi_t}, \quad (2)$$

where $\Delta S_0 = \epsilon \ln(1 + L_z)$ is the initial entropy difference between the top and bottom of the atmosphere and $c_P = \gamma(\gamma - 1)^{-1}$ is the specific heat at constant pressure. The profiles of ν and χ are constant with time, and Ra at the bottom of the atmosphere is greater than Ra_{top} by a factor of $e^{2n\rho}$. This formulation leaves the thermal conductivity, $\kappa = \rho \chi$, and the dynamic viscosity, $\mu = \rho \nu$, free to evolve as the density profile changes. Henceforth, when we use Ra , we are referring to Ra_{top} .

We evolve the Fully Compressible Navier-Stokes equations,

$$\frac{\partial \ln \rho}{\partial t} + \nabla \cdot \mathbf{u} = -\mathbf{u} \cdot \nabla \ln \rho, \quad (3)$$

$$\frac{\partial \mathbf{u}}{\partial t} + \nabla T - \nu \nabla \cdot \bar{\boldsymbol{\sigma}} - \bar{\boldsymbol{\sigma}} \cdot \nabla \nu = -\mathbf{u} \cdot \nabla \mathbf{u} - T \nabla \ln \rho + \mathbf{g} + \nu \bar{\boldsymbol{\sigma}} \cdot \nabla \ln \rho, \quad (4)$$

$$\begin{aligned} \frac{\partial T}{\partial t} - \frac{1}{c_V} (\chi \nabla^2 T + \nabla T \cdot \nabla \chi) &= -\mathbf{u} \cdot \nabla T - (\gamma - 1) T \nabla \cdot \mathbf{u} \\ &\quad + \frac{1}{c_V} (\chi \nabla T \cdot \nabla \ln \rho + \nu [\bar{\boldsymbol{\sigma}} \cdot \nabla] \cdot \mathbf{u}), \end{aligned} \quad (5)$$

with the viscous stress tensor given by

$$\sigma_{ij} \equiv \left(\frac{\partial u_i}{\partial x_j} + \frac{\partial u_j}{\partial x_i} - \frac{2}{3} \delta_{ij} \nabla \cdot \mathbf{u} \right). \quad (6)$$

Taking an inner product of (4) with $\rho \mathbf{u}$ and adding it to $\rho c_V \times (5)$ reveals the full energy equation,

$$\frac{\partial}{\partial t} \left(\rho \left[\frac{|\mathbf{u}|^2}{2} + c_V T + \phi \right] \right) + \nabla \cdot (\mathbf{F}_{\text{conv}} + \mathbf{F}_{\text{cond}}) = 0, \quad (7)$$

where $\mathbf{F}_{\text{conv}} \equiv \mathbf{F}_{\text{enth}} + \mathbf{F}_{\text{KE}} + \mathbf{F}_{\text{PE}} + \mathbf{F}_{\text{visc}}$ is the convective flux and $\mathbf{F}_{\text{cond}} = -\kappa \nabla T$ is the conductive flux. The individual contributions to \mathbf{F}_{conv} are the enthalpy flux, $\mathbf{F}_{\text{enth}} \equiv \rho \mathbf{u} (c_V T + P/\rho)$; the kinetic energy flux, $\mathbf{F}_{\text{KE}} \equiv \rho |\mathbf{u}|^2 \mathbf{u}/2$; the potential energy flux, $\mathbf{F}_{\text{PE}} \equiv \rho \mathbf{u} \phi$ (with $\phi \equiv -gz$); and the viscous flux, $\mathbf{F}_{\text{visc}} \equiv -\rho \nu \mathbf{u} \cdot \bar{\boldsymbol{\sigma}}$. Understanding how each of these fluxes interact is crucial in characterizing convective heat transport.

We utilize the Dedalus¹ [7] pseudospectral framework to time-evolve (3)-(5) using an implicit-explicit (IMEX),

third-order, four-step Runge-Kutta timestepping scheme RK443 [8]. We decompose our thermodynamic variables such that $T = T_0 + T_1$ and $\ln \rho = (\ln \rho)_0 + (\ln \rho)_1$, and the velocity $\mathbf{u} = u \hat{x} + v \hat{y} + w \hat{z}$. In our 2D runs, $v = 0$. Subscript 0 variables, set by (1), have no time derivative and vary only in z . Variables are time-evolved on a dealiased Chebyshev (vertical) and Fourier (horizontal, periodic) domain in which the physical grid dimensions are 3/2 the size of the coefficient grid. Domain sizes range from 64x256 coefficients at the lowest values of Ra to 1024x4096 coefficients at $\text{Ra} > 10^7$ in 2D, and from 64x128² to 256x512² in 3D. By using IMEX timestepping, we implicitly step the stiff linear acoustic wave contribution and are able to efficiently study flows at high (~ 1) and low ($\sim 10^{-4}$) Ma. Our equations take the form of the FC equations in [9], extended to include ν and χ which vary with depth, and we follow the approach there. This IMEX approach has been successfully tested against a nonlinear benchmark of the compressible Kelvin-Helmholtz instability [10].

We impose impenetrable, stress free, fixed temperature boundary conditions at the top and bottom of the domain such that $w = \partial_z u = T_1 = 0$ at $z = \{0, L_z\}$. T_1 is initially filled with random white noise whose magnitude is infinitesimal compared to T_0 and ϵ . We filter this noise spectrum in coefficient space, such that only the lower 25% of the coefficients have power. We non-dimensionalize our computational domains by setting all thermodynamic variables to unity at $z = L_z$ choosing $R = T_t = \rho_t = 1$. By this choice, the non-dimensional length scale is the inverse temperature gradient scale and the timescale is the isothermal sound crossing time, τ_I , of this unit length. Meaningful convective dynamics occur on timescales of the atmospheric buoyancy time, $t_b = \tau_I \sqrt{L_z/gc}$. All reported results are taken from time averages over many t_b beginning $\{100, 40\}t_b$ after the start of our {2D, 3D} simulations in order to assure our results are not biased by the convective transient.

RESULTS & DISCUSSION

Solutions were time-evolved until a long time average of the fluxes showed little variance with depth. By performing a linear stability analysis, we determined that the onset of convection occurs at $\text{Ra}_{\text{crit}} = \{11.15, 10.06, 10.97, 10.97\}$ for $\epsilon = \{1.0, 0.5, 10^{-4}, 10^{-7}\}$, respectively.

We measure the adiabatic Mach number ($\text{Ma} = |\mathbf{u}|/\sqrt{\gamma T}$). We find that Ma is a strong function of ϵ and a weak function of Ra . In our 2D runs, when $\text{Ma} < 1$ we observe a scaling law of $\text{Ma}(\text{Ra}, \epsilon) \propto \epsilon^{1/2} \text{Ra}^{1/4}$. This relation breaks down as the mean Ma approaches 1 (see Fig. 1). This transition occurs near $\text{Ra}/\text{Ra}_{\text{crit}} \approx \{10^2, 10^3\}$ for $\epsilon = \{1, 0.5\}$. In our limited 3D runs, Ma appears to be a function of ϵ alone, with $\text{Ma} \propto \epsilon^{1/2}$, so at high

¹ <http://dedalus-project.org/>

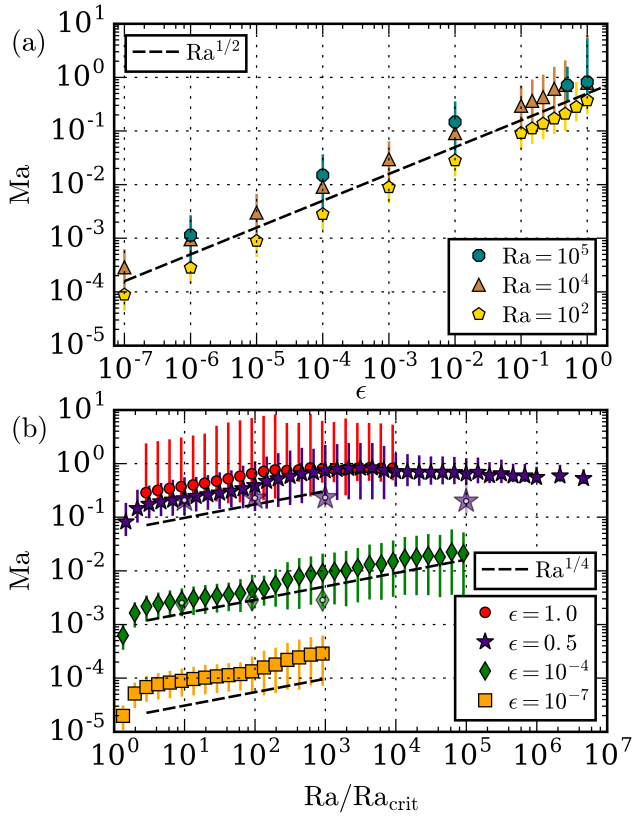


FIG. 1. The mean adiabatic Mach number of long-time-averaged profiles is shown. Error bars show the full range of Ma over the depth of the atmosphere. (a) Ma, at various values of Ra, is plotted as a function of ϵ . (b) Ma, at various values of ϵ , is plotted as a function of $\text{Ra}/\text{Ra}_{\text{crit}}$. Larger symbols with white dots designate 3D runs.

Ra , $\text{Ma}_{3D} < \text{Ma}_{2D}$. The value of ϵ also sets the size of the evolved thermodynamic fluctuations, such that $T_1/T_0 \propto \epsilon$ and $\rho_1/\rho_0 \propto \epsilon$. These fluctuations are very small when ϵ and Ma are small, but can be $O(1)$ for values of ϵ near 1.

Low Ma flows (e.g., $\epsilon = 10^{-4}$) display the classic narrow downflow and broad upflow lanes of stratified convection (Fig. 2a). At high Ma (e.g., $\epsilon = 0.5$), bulk thermodynamic structures are similar but shock systems form in the upper atmosphere near downflow lanes for sufficiently large values of ϵ and Ra (Fig. 2b,c). Similar shock phenomena were reported in both two [4] and three [12] dimensional polytropic simulations previously. As Ra is increased to large values (Fig. 2c), thermodynamic structures no longer span the whole domain but rather break up into small eddies which traverse the domain multiple times before diffusing. Our choice of fixed-temperature, stress free boundary conditions allows the flux at the boundaries to vary, while also allowing for mean horizontal velocity profiles along the boundaries (winds). We find these windy convective states, reminis-

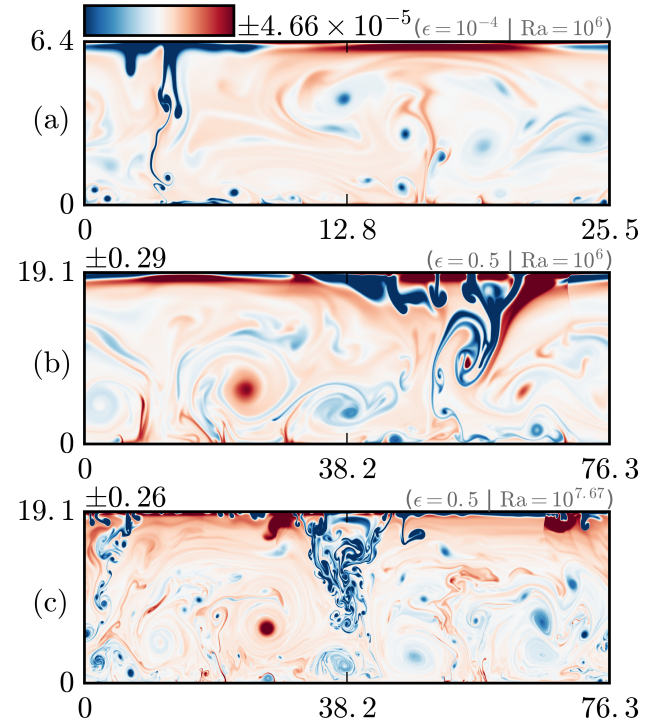


FIG. 2. Characteristic entropy fluctuations in evolved 2D flows roughly $140t_b$ after the start of simulations. The time- and horizontally-averaged profile is removed in all cases. (a) A low Ma flow at moderate Ra. (b) A high Ma flow at the same Ra as in (a). (c) a high Ma flow at high Ra. Shock systems can be seen in the upper atmosphere of the high Ma flows, for example at $(x, z) \approx (70, 15 - 19)$ in (b) and $(x, z) \approx (65, 17 - 19)$ in (c).

cent of similar states in RB convection [11], at $\epsilon = 10^{-4}$ for high values of Ra. Roll states (Fig. 2a) with high convective transport alternate with windy states of lower transport.

The efficiency of convection is quantified by the Nusselt number (Nu). Nu is well-defined in RB convection as the total flux normalized by the steady-state conductive flux [13, 14]. In stratified convection Nu is more difficult to define, and we use a modified version of a traditional stratified Nusselt number [1, 3],

$$\text{Nu} \equiv \frac{\langle F_{\text{conv},z} + F_{\text{cond},z} - F_A \rangle}{\langle F_{\text{cond},z} - F_A \rangle} = 1 + \frac{\langle F_{\text{conv},z} \rangle}{\langle F_{\text{cond},z} - F_A \rangle} \quad (8)$$

where $F_{\text{conv},z}$ and $F_{\text{cond},z}$ are the z-components of \mathbf{F}_{conv} and \mathbf{F}_{cond} , and $\langle \rangle$ are volume averages. $F_A \equiv -\langle \kappa \rangle \partial_z T_{\text{ad}}$ is the conductive flux of the proper corresponding adiabatic atmosphere. For a compressible ideal gas in hydrostatic equilibrium, $\partial_z T_{\text{ad}} \equiv -g/c_P$ [15]. It is important to measure the evolved value of $\langle \kappa \rangle = \langle \rho \chi \rangle$, which is nearly κ_0 when ϵ is small but can change appreciably for large values of ϵ . In incompressible Boussinesq convection, where $\nabla S = 0$ only when $\nabla T = 0$, this definition

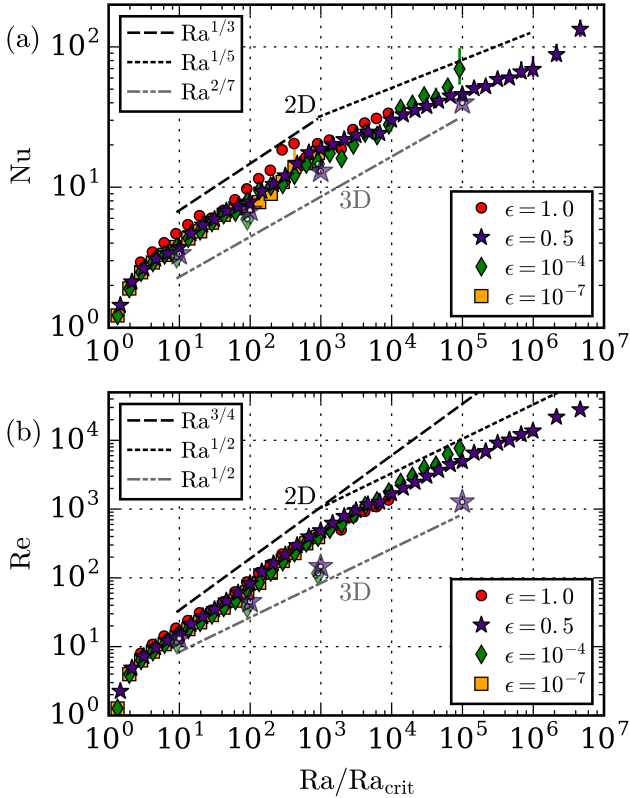


FIG. 3. Flow properties at high and low ϵ . (a) Nu vs. $\text{Ra}/\text{Ra}_{\text{crit}}$. Errors bars indicate the variance of Nu with depth; large error bars indicate a poorly converged solution. (b) Re vs. $\text{Ra}/\text{Ra}_{\text{crit}}$. Re is measured at the midplane of the atmosphere. Larger symbols with white dots designate 3D runs.

reduces to the traditional definition of the Nusselt number [13, 14].

The variation of Nu with Ra is shown in Fig. 3a. We find that the Nu depends primarily on Ra , not on ϵ , except where dynamical regimes change. In 2D and at low to moderate Ra , $\text{Nu} \propto \text{Ra}^{1/3}$ regardless of ϵ , reminiscent of scaling laws in classical Rayleigh-Bénard theory [16]. As the flow becomes supersonic, $\text{Nu} \propto \text{Ra}^{1/5}$. 2D runs at $\text{Ra} > 10^3 \text{Ra}_{\text{crit}}$ and $\epsilon = 10^{-4}$ exhibit windy convective states. In these runs, the system is in flux equilibrium only when time averaged over roll states and windy states. A long time average over both of these states produces a flat flux profile which can be sensibly analyzed, but the presence of these time-dependent states makes it difficult to equilibrate these higher Ra cases. It is also important to note that the value of Nu is heavily dependent upon the specific thermodynamic structures of the solution, as double roll states will transport heat more efficiently than single roll states, and slight changes in Ra can result in a simulation latching on to one solution or the other. In our limited 3D runs, it appears that $\text{Nu} \propto \text{Ra}^{2/7}$, a classic scaling law seen in RB studies [13].

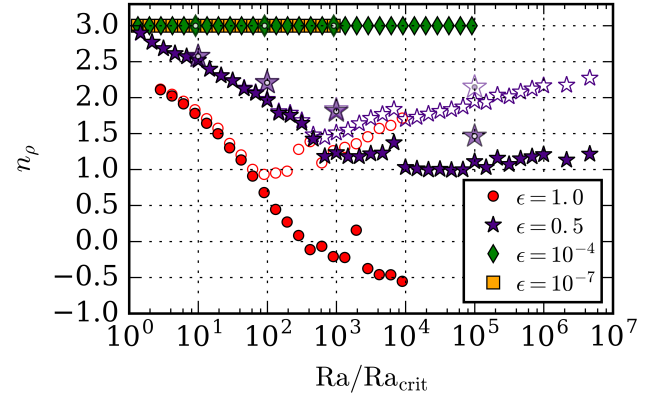


FIG. 4. Solid symbols show the density contrast measured in density scale heights between the upper and lower boundary, $n_\rho = \ln[\rho(z=0)/\rho(z=L_z)]$. Empty symbols show $n_\rho = \ln[\max(\rho)/\min(\rho)]$. At low ϵ the evolved n_ρ is close to the initial conditions of $n_\rho = 3$. At high ϵ , the density stratification decreases. Once the mean Ma approaches 1 (at $\text{Ra}/\text{Ra}_{\text{crit}} \approx \{10^2, 10^3\}$ for $\epsilon = \{1, 0.5\}$ as in Fig. 1b), density inversions form within the thermal boundary layers. Larger symbols represent 3D runs.

The rms Reynolds number ($\text{Re} = |\mathbf{u}|L_z/\nu$) and Peclet number ($\text{Pe} = \text{Pr} \text{Re}$) compare the importance of advection to diffusion in the evolved convective state. For $\text{Pr} = 1$, such as in this work, $\text{Pe} = \text{Re}$. Our choice of $\{\nu, \chi\} \propto \rho_0^{-1}$ drastically changes the value of Re between the top and bottom of the atmosphere. We report values of Re at the midplane ($z = L_z/2$) of the atmosphere in Fig. 3b. Largely we find that Ra and Pe depend on Ra , but not ϵ , except when the flow states change. In 2D and at low Ra , $\text{Re} \propto \text{Ra}^{3/4}$. When the flows become supersonic, this scaling gives way to $\text{Re} \propto \text{Ra}^{1/2}$. In our limited 3D runs, the scaling of Re is $\text{Re} \propto \text{Ra}^{1/2}$, consistent with the supersonic results.

In the evolved state, the flows change the density stratification, as shown in Fig. 4. We find that supersonic flows support persistent density inversions (empty symbols) in the boundary layers, as was reported by [17]. We find this in 2D and 3D. Surprisingly, the evolved n_ρ is always less than the initial $n_\rho = 3$, and turbulent pressure support plays a larger role than atmospheric slumping. The agreement of Nu , Re across ϵ (Fig. 3), particularly at low Ra in which all four of our cases collapse onto a single power law, is striking in light of the vastly different evolved stratifications felt by the flows.

In summary, we have found that the evolved flow properties of stratified, compressible convection scale in a manner reminiscent of RB convection. We argue that polytropically stratified atmospheres are the natural extension of the RB problem with an additional control parameter, ϵ , whose primary role is to set the Ma of the flows. We show that other properties of the evolved solutions (Nu , Re) are nearly identical at vastly different

values of ϵ , except for where there is a transition between the subsonic and supersonic regimes. We also see that Nu scales similarly in 3D and 2D, and that Ma in 3D solutions seems to be a function of ϵ alone, allowing for simple specification of the evolved Ma using input parameters.

We have observed interesting phenomena, such as time-dependent oscillating shearing “windy” states in our 2D simulations. Unlike in RB [11], our solutions with windy states have transport which scales in line with our non-windy solutions. Furthermore, the stratification of these polytropic atmospheres evolves in a complex manner. Future work should aim to understand the importance of stratification on convective heat transport and other flow properties.

Our studies here will serve as a foundation both for understanding and comparing heat transport in stratified convection to that in RB convection [13], and for future studies of transport in stratified convection. These results can be used to determine if simplified equation sets, such as the anelastic equations, carry heat in the same manner as the FC equations. This work will also be useful in coming to understand more realistic systems, such as rapidly rotating atmospheres [19], atmospheres bounded by stable regions [20], or regions with realistic profiles of κ .

acknowledgements

EHA acknowledges the support of the University of Colorado’s George Ellery Hale Graduate Student Fellowship. This work was additionally supported by NASA LWS grant number NNX16AC92G. Computations were conducted with support by the NASA High End Computing (HEC) Program through the NASA Advanced Supercomputing (NAS) Division at Ames Research Center on Pleiades with allocations GID s1647 and GID g26133. We thank Jon Aurnou, Axel Brandenburg, Keith Julien, Mark Rast, and Jeff Oishi for many useful discussions. We also thank the two anonymous referees whose careful comments greatly improved the quality of this letter.

-
- [1] E. Graham, Journal of Fluid Mechanics **70**, 689 (1975).
 - [2] K. L. Chan, S. Sofia, and C. L. Wolff, Astrophys. J. **263**, 935 (1982).
 - [3] N. E. Hurlburt, J. Toomre, and J. M. Massaguer, Astrophys. J. **282**, 557 (1984).
 - [4] F. Cattaneo, N. E. Hurlburt, and J. Toomre, ApJL **349**, L63 (1990).
 - [5] F. Cattaneo, N. H. Brummell, J. Toomre, A. Malagoli, and N. E. Hurlburt, Astrophys. J. **370**, 282 (1991).
 - [6] N. H. Brummell, N. E. Hurlburt, and J. Toomre, Astrophys. J. **473**, 494 (1996).
 - [7] K. Burns, G. Vasil, D. Lecoanet, J. Oishi, and B. Brown, *Dedalus: Flexible framework for spectrally solving differential equations*, Astrophysics Source Code Library (2016), 1603.015.
 - [8] U. M. Ascher, S. J. Ruuth, and R. J. Spiteri, Applied Numerical Mathematics **25**, 151 (1997).
 - [9] D. Lecoanet, B. P. Brown, E. G. Zweibel, K. J. Burns, J. S. Oishi, and G. M. Vasil, Ap. J. **797**, 94 (2014), 1410.5424.
 - [10] D. Lecoanet, M. McCourt, E. Quataert, K. J. Burns, G. M. Vasil, J. S. Oishi, B. P. Brown, J. M. Stone, and R. M. O’Leary, MNRAS **455**, 4274 (2016), 1509.03630.
 - [11] D. Goluskin, H. Johnston, G. R. Flierl, and E. A. Spiegel, Journal of Fluid Mechanics **759**, 360 (2014).
 - [12] A. Malagoli, F. Cattaneo, and N. H. Brummell, ApJL **361**, L33 (1990).
 - [13] H. Johnston and C. R. Doering, Physical Review Letters **102**, 064501 (2009), 0811.0401.
 - [14] J. Otero, R. W. Wittenberg, R. A. Worthing, and C. R. Doering, Journal of Fluid Mechanics **473**, 191 (2002).
 - [15] E. A. Spiegel and G. Veronis, Astrophys. J. **131**, 442 (1960).
 - [16] E. M. King, S. Stellmach, and J. M. Aurnou, Journal of Fluid Mechanics **691**, 568 (2012).
 - [17] A. Brandenburg, K. L. Chan, Å. Nordlund, and R. F. Stein, Astronomische Nachrichten **326**, 681 (2005), astro-ph/0508404.
 - [18] G. Ahlers, S. Grossmann, and D. Lohse, Rev. Mod. Phys. **81**, 503 (2009).
 - [19] K. Julien, E. Knobloch, A. M. Rubio, and G. M. Vasil, Physical Review Letters **109**, 254503 (2012).
 - [20] N. E. Hurlburt, J. Toomre, and J. M. Massaguer, Astrophys. J. **311**, 563 (1986).